Cryo-EM structures reveal two distinct conformational states in a picornavirus cell entry intermediate.

Pranav N.M. Shah[1†], David J. Filman[1], Krishanthi S. Karunatilaka[1], Emma L. Hesketh[2], Elisabetta Groppelli[3#], Mike Strauss[4], James M. Hogle[1*]

Affiliations

1. Department of Biological Chemistry and Molecular Pharmacology, Harvard Medical School, 240 Longwood Medical Ave., Boston, MA 02115, USA.

2. Astbury Centre for Structural Molecular Biology, School of Molecular & Cellular Biology, Faculty of Biological Sciences, University of Leeds, Leeds LS2 9JT, UK

3. School of Molecular and Cellular Biology, Faculty of Biological Sciences, University of Leeds, Leeds LS2 9JT, UK

4. Department of Anatomy and Cell Biology, McGill University, 3640 University St., Montreal, QC H3A 0C7, Canada

†*Present Address: The Division of Structural Biology, The Henry Wellcome Building for Genomic Medicine, Roosevelt Drive, Oxford, OX3 7BN*

#*Present Address: Institute of Infection and Immunity, St George's, University of London, Cranmer Terrace, Tooting, London SW17 0RE, UK*

*Correspondence to James M. Hogle: james_hogle@hms.harvard.edu

Keywords: Poliovirus, cryo-EM, virus entry

AUTHOR SUMMARY

Nonenveloped viruses need to provide mechanisms that allow their genomes to be delivered across membrane. This process remains poorly understood. For enterovirus such as poliovirus, genome delivery involves a program of conformational changes that include expansion of the particle and externalization of two normal internal peptides, VP4 and the VP1 N-terminus, which then insert into the cell membrane, triggering endocytosis and the creation of pores that

facilitate the transfer of the viral RNA genome across the endosomal membrane. This manuscript describes five high-resolution cryo-EM structures of altered poliovirus particles that represent a number of intermediates along this pathway. The structures reveal several surprising findings, including the discovery of a new intermediate that is expanded but has not yet externalized the membrane interactive peptides, the clear identification of a unique exit site VP1 N-terminus, the demonstration that the externalized VP1 N-terminus partitions between two different sites in a temperature-dependent fashion, direct visualization of an amphipathic helix at the N-terminus of VP1 in an ideal position for interaction with cellular membranes, and the observation that a significant portion of VP4 remains inside the particle and accounts for a feature that had been previously ascribed to part of the viral RNA. These findings represent significant additions to our understanding of the cell entry process of an important class of human pathogens.

ABSTRACT

The virions of enteroviruses such as poliovirus undergo a global conformational change after binding to the cellular receptor, characterized by a 4% expansion, and opening of holes at the two and quasi-three-fold symmetry axes of the capsid. The resultant particle is called a 135S particle or A-particle and is thought to be on the pathway to a productive infection. Previously published studies have concluded that the membrane interactive peptides, namely VP4 and the N-terminus of VP1, are irreversibly externalized in the 135S particle. However, using established protocols to produce the 135S particle, and single particle cryo-electron

55 microscopy methods, we have identified at least two unique states that we call the
56 early and late 135S particle. Surprisingly, only in the “late” 135S particles have
57 detectable levels of the VP1 N-terminus trapped outside the capsid. Moreover, we
58 observe a distinct density inside the capsid that can be accounted for by VP4 that
59 remains associated with the genome. Taken together our results conclusively
60 demonstrate that the 135S particle is not a unique conformation, but rather a family
61 of conformations that could exist simultaneously.
62

63 **INTRODUCTION**

64 Poliovirus is a small (~30nm) non-enveloped, positive sense, single-stranded RNA
65 virus. It belongs to the genus Enterovirus of the Picornaviridae, and is the
66 causative agent of poliomyelitis [1]. The icosahedral capsid of the virus, which is
67 made of four proteins, namely VP1, VP2, VP3, and VP4, encloses the viral genome
68 [2]. The capsid is structurally similar to other members of the family such as
69 Rhinovirus, Coxsackievirus A16, and Enterovirus 71 and Enterovirus D68, the
70 latter three having caused recent epidemics of hand-foot-and-mouth disease, and
71 even flaccid paralysis in China and the United States[1,3,4]. Therefore, studies on
72 poliovirus are not only crucial to support the global effort to eradicate poliovirus,
73 but also to tackle important emerging pathogens.
74

75 Poliovirus entry into cells is initiated when the virus interacts with its receptor,
76 CD155, also known as poliovirus receptor (PVR) [5], an immunoglobulin-like
77 molecule which is expressed at the intercellular junctions of epithelial cells [6].

Receptor engagement is concomitant with the loss of the “pocket factor” [7], a stabilizing ligand [8] that binds in the hydrophobic core of VP1 [9]. Structurally, receptor binding results in an icosahedral expansion of the capsid by 4% [10], resulting in a 135S, or A- particle [11-14]. These particles are metastable, infectious [15,16] and RNA-containing. Therefore, it is thought that the 135S particle represents a critical step along the pathway to infection [16]. Unlike mature native virions (160S particles), whose capsids form a closed surface, the expanded 135S particles have holes in the capsid at the icosahedral 2-fold and quasi-3-fold axes. These openings permit the externalization of the hydrophobic, membrane-interactive N-terminal extension of capsid protein VP1 [11,14,17] and the myristoylated protein, VP4 [18]. *In vitro* studies with model membranes have shown that these polypeptide chains are responsible for anchoring the virus to the host cell membrane [11,19]. Earlier tomographic studies from our group demonstrated umbilical connections between the virus and receptor decorated liposomal membranes [20] were wide enough to accommodate single-stranded RNA genome. This could be the manner in which the genome is protected from the degradative effects of RNases [21]. However, the molecular and structural underpinnings of this process still remain elusive.

In the present study we report five high-resolution reconstructions of the 135S uncoating intermediate particles, with refined atomic models for four of them. Taken together, our results describe a multi-step model for picornavirus capsid uncoating and subsequent steps in genome translocation.

RESULTS

Three structures produced by incubation with mAb

Initially we set out to investigate the structure of the “breathing” poliovirus particle. Previous studies showed that native poliovirions, when incubated at 37˚C (but not at 25˚C), transiently expose membrane-interactive polypeptides VP4 and the N-terminus of VP1 [22]. These two exposed polypeptides could be trapped outside the capsid by specific antibodies, some of which neutralized infectivity [22]. The release of the antibodies by freeze-thaw restored infectivity, demonstrating that the process was reversible [22]. An early attempt to characterize the breathing particle trapped using an Fab that recognized residues 39-55 of VP1 [23] produced a low-resolution structure [24]. This structure revealed an RNA-containing virus particle whose capsid was trapped in an icosahedrally symmetric expanded state that was purported to be different from previously reported expanded forms of poliovirus. Weak and poorly ordered density located above the icosahedral 2-fold hole was attributed to peptide-bound Fab molecules getting "stuck" in random orientations when the VP1 N-terminus was partially withdrawn into the particle interior [24].

In the current study we have leveraged improvements in EM and computer hardware, data collection software, and image processing pipelines to re-examine with higher detail the antibody-trapped states relevant to the uncoating process, starting with the poliovirus "breathing" particle. This particle was produced by

incubating native poliovirus with a commercially available monoclonal antibody (kind gift from Quidel Corp.) that was raised against a peptide corresponding to VP1 residues 42-55 (PALTAVETGATNPL). Although the antibodies used in this and previous studies recognize the same region of the N-terminus of VP1, this antibody differs from the one previously used, which is no longer available. Thus, in contrast to the earlier antibody which showed significant binding when incubating virus with the Fab, we could only obtain significant decoration of particles using the intact monoclonal antibody provided by Quidel. Single particle screening cryo-EM experiments were conducted to determine conditions that would yield the greatest number of virus-mAb complexes. An optimal number of complexes was observed after a 90-minute incubation of the virus at 39˚C with intact (bivalent) antibody.

Under those conditions, three main structural classes were obtained (Fig. 1a), each containing roughly one-third of the usable particle images. Class 1 was not labeled by antibodies and was indistinguishable from previously solved 160S native virus [2], having an RNA core; VP4 and the N-terminus of VP1 bound on the inner surface of the capsid; and a closed protein shell that lacked large holes (left column, Fig. 1a). Classes 2 and 3 both consisted of capsids that were expanded by about 4%, with large holes at the 2-fold axes. The class 2 particles appeared to contain a full complement of RNA (middle column, Fig. 1a), whereas class 3 appeared similar to previously-studied 80S empty capsids [10,25,26] (rightmost

column, Fig. 1a), which lack RNA, VP4, order in residues 1-68 of VP1, and which have either unobstructed or partially obstructed holes at the quasi-3-fold axes.

The 80S-like class. In the icosahedral reconstructions of the class 3 particles, the density for the Fab portion of the bound antibody (for simplicity we will refer to this here and in subsequent sections as the Fab) was a flat roundish feature whose connection with the capsid was not directly apparent (rightmost column, Fig. 1a). This density enclosed only the lower half of the Fab and was only visible at a much lower contour level than the capsid protein, suggesting both low occupancy, and variability in the position and angle of the Fab with respect to the virus. The position of the Fab, over the 2-fold hole, was similar to one of two sites for Fab binding in the low-resolution structure of an 80S-Fab complex described previously [27].

To further assess the interaction of the Fab with the capsid, we performed an asymmetric focused classification on 542,460 asymmetric units of the virus, using a cylindrical mask that enclosed the 2-fold axis of the capsid as well as the Fab. While the capsid was resolved to 4.2A in the icosahedrally averaged maps, the focused class in (Fig. 1b.) resolved to 6.5A. This class had a distinct tube-like density extending from above the VP2 helix (residues 90-100) at the 2-fold axis to the underside of the Fab (Fig. 1b). We interpret this density to be the N-terminus of VP1.

135S-like particles (m135). Class 2 (which we will call m135) was the most interesting of the 3 classes (Fig. 2 and middle column of Fig. 1a), as it shared several of the physical characteristics of the canonical 135S particles. The m135 reconstruction was resolved to 2.8Å resolution in the capsid region, after masking and "sharpening" (see Methods) (Table S1, Fig. S1), and a detailed atomic model was constructed and refined for ordered amino acids in capsid proteins VP1, VP2, and VP3. Like a canonical 135S particle, the m135 reconstruction includes a significant central density for the RNA (but whose apparent icosahedral symmetry is an artefact of the calculation), lacks VP4 on the inner surface of the capsid, and has an expanded capsid with holes at the 2-fold and quasi-3-fold axes (middle column Fig. 1a). In this structure and in all of the remaining 135S structures described below, the pocket factor is missing from the hydrophobic pocket of VP1 [9]. Similar to 135S-like particles for other enteroviruses [28,29], this structure has an additional portion of the N-terminal extension of VP1 (residues 64-69) that is ordered, and extends outward along the quasi-3-fold axis (Fig. 2b-d).

The density for the Fab is diffuse and rod-shaped, stretching between two 2-fold-related copies of the quasi-3-fold hole (Fig. 2a and middle column of Fig. 1a). The rod-like density feature is only evident above the noise level for the lower half of the Fab, which suggests variability in the position and orientation of the Fab. The weakness of the ordered Fab density (in the icosahedrally averaged maps) is consistent with a model in which specific Fab binding (to residues 42-55 of the VP1

192 N-terminus) at some of the quasi-3-fold sites near the virus surface is precluded
193 by steric conflicts with previously bound Fabs.
194
195 In the high-resolution m135 structure, we see two general categories of structural
196 change relative to native virus. One category corresponds to movement of the
197 beta barrels of the major capsid proteins, VP1-3, away from one another when the
198 capsid expands. As a consequence, several polypeptide segments (which, in
199 native 160S virus, stabilize the "closed" capsid arrangement) detach from their
200 neighbors and become disordered. On the inner surface of the capsid, these
201 segments include VP4 and portions of the N-terminal extensions of VP1 and VP2.
202 On the outer surface of the capsid, these segments include all C-termini of VP1,
203 VP2, and VP3, as well as loops extending from the beta-barrel cores of VP1 and
204 VP2 (see below). The general pattern of beta barrel shifts and polypeptide chain
205 disordering that occurs upon the expansion of poliovirus has previously been
206 analyzed [10,25,26,30]. A specific listing of ordered and disordered residues is
207 tabulated (see Table S2) for the m135 atomic model, and for the three other atomic
208 models described below.
209
210 The second, particularly interesting, set of structural changes involves the
211 polypeptide segments that contact the VP1 N-terminus as it exits through the
212 quasi-3-fold hole. Notably, the GH loop of VP3 (residues 176-185) uncoils,
213 changing from a compact structure that plugs the quasi-3-fold in virions into a more
214 extended structure that leaves room for residues 62-68 (residues 1-61 were not

modellable in this density) of VP1 to thread through the quasi-3-fold (Fig. 2c-d). Additionally, the "bottom" loop of VP2 (residues 26-58), which encircles the bottom of the VP2 beta barrel, rearranges at its tip (residues 43-55) to move out of the way of the externalizing VP1 N-terminus (Fig. 2d-e). Finally, a portion of the GH loop of VP1 (residues 216-236) rearranges to facilitate the externalization of the VP1 N-terminus; and the C-terminal extension of VP2 (residues 262-272) retracts from its position on the outside of the virion to bind to the inner surface of the capsid (Fig. 2f). The movement of the VP1-3 beta barrels is strikingly consistent with all of the 135S structures reported here and in those previously published for poliovirus and other enteroviruses [17,25,30-32](see ordered residue lists, Table S2). In particular, the four key contact areas (Fig. 2c-f) either change their conformation or become disordered as a result of the 160S-to-135S conversion.

Finally, we considered the possibility that our antibody-trapped “breathing” particles would regain infectivity if the antibody were released by freeze-thawing, as was reported in the original report of “breathing” of poliovirus [22]. To test this possibility, virus samples were incubated with VP1 antibodies either at 39ºC (where breathing is expected) or 25˚C (where breathing is not expected) for 1.5 h (the same as for the EM experiment) and immunoprecipitated with Protein A/G coated magnetic beads at room temperature. Unbound virus was washed away, and the bound virus was released from the beads by freeze-thawing the solution. Next, the released virus was serially diluted and used to infect naïve Vero cells. Greater cytopathic effect was observed in virus particles retrieved from incubating

238 the virus with the antibody at higher temperature than the virus particles retrieved
239 from the room temperature incubation (Fig S2a-b). This suggests that some of the
240 antibody-bound particles must have retained a full or nearly full complement of
241 proteins (presumably including VP4) and remained infectious, even when
242 accounting for non-specific binding of native virus to the antibody.
243
244 **Comparison of m135 particles with "canonical" 135S particles.**
245
246 Historically, three methods were used to convert 160S virus to 135S particles, and
247 the resulting particles were not distinguishable by any of the tests then available.
248 One method involved the binding of virus by the poliovirus receptor at the cell
249 surface at 37 ˚C in a natural infection [11-13]; the second involved incubation of
250 virus with the soluble ectodomain of the receptor at 37˚C [33,34]; and the third
251 involved heating 160S particles at 50˚C in the presence of divalent cations that
252 stabilize the meta-stable 135S intermediate [11,15,35]. To assess whether or not
253 the m135 particle was indeed 135S-like, we decided to solve cryo-EM structures
254 for both the soluble-receptor-triggered and heat-triggered 135S particles.
255 Consistent with our "standard recipes" for producing 135S particles [8,15], we
256 incubated native virus for 3 min, either with solubilized PVR at 37˚C, or alone at
257 50˚C. Receptor-triggered and heat-triggered 135S structures (designated "r135"
258 and "h135", respectively) were solved at 3.2Å resolution (after density-based
259 masking and sharpening) (Table S1, Fig. S1b-c).
260

As expected, the capsids of both r135 and h135 were expanded by 4%, with holes at the 2-fold axes, were full of RNA, and failed to show well-ordered native-like VP4 pentamers lying flat on the inner surface of the capsid (Fig. 3a). The r135 and h135 structures were identical, except for the occasional shift, by one or two residues along the polypeptide chain, where an order-to-disorder transition occurred. The set of "buildable" residues whose main chain atoms could be included in each atomic model are listed in Table S2.

Surprisingly, both r135 and h135 maps lacked a visible extension of the VP1 N-terminus through the quasi-3-fold hole, which was supposed to be the structural hallmark of a 135S particle, according to the literature [11,17,30,36]. In both cases, residue 69 was the first ordered residue of VP1; residues 43-53 of the bottom loop of VP2 (which supports the VP1 N-terminus) were disordered; and the quasi-3-fold hole was partially blocked by the GH loop of VP3 (Fig. 3b). The lower portion of the loop was similar to that seen in native 160S virus (Fig. 3c), but the upper portion was different from either the 160S structure or previously described 135S structures in which the VP1 N-termini were exposed. In short, while the literature[17,29,32] (and our own experience [14]) had led us to expect a 3 min incubation to produce an expanded particle with the VP1 N-termini extended, the 3 min incubation in this study produced an expanded and fenestrated capsid in which most or all of the VP1 N-terminus remained inside the capsid. Therefore, we propose that the category of particles that was previously called “135S” most likely consists of distinct states, namely, an “early state”, wherein the capsid has

284 undergone an expansion but most copies of the VP1 N-terminus are on the inside
285 of the capsid and the quasi-3-fold hole still remains blocked, and a subsequent
286 “late state”, characterized by the opening of the quasi 3-fold hole and the
287 emergence of many copies of the VP1 N-termini through them. In support of this
288 possibility, a careful re-reading of the literature [9,15,22,36] showed that 135S
289 particles with extended N-termini were typically detected only after extensive
290 purification and/or prolonged incubations.
291
292 **Receptor-induced 135S particles incubated with mAb at 25˚C**
293
294 To test our hypothesis, that VP1 N-termini (from expanded particles) become
295 externalized after an extended time, we followed the method described in Tsang
296 et al [37], first incubating the virus with receptor for 3 mins at 37˚C, followed by a
297 1hr incubation with antibody at 25˚C. This protocol was carried out twice, once with
298 a smaller "screening" data set, and once with a larger one. Data collection
299 parameters are summarized in Table S1.
300
301 As predicted, incubation of the pre-formed "early 135S particle" with antibody for
302 1hr at 25˚C did decorate the virus particles with Fab-shaped density features. (Fig.
303 4a). Surprisingly, the Fab portions of the antibody molecules did not bind at quasi-
304 3-fold positions, to produce a low-level rod-shaped density, such as that seen in
305 the m135 map (Fig. 2a and Fig 1a middle column). Instead, the Fab density in the
306 icosahedrally-averaged map was poised above the 2-fold hole. Its position was

similar to that of the much weaker hemispherical density in the decorated 80S particles (rightmost column, Fig. 1a). However, in the new "r135+m25" reconstruction, density for the Fab was much better ordered, with the upper half of the Fab domain visible, and separated from the lower half by an appropriately placed gap in the density between subdomains (Fig. 4b). Unlike the decorated 80S map, where the Fab may have been freely spinning around the viral 2-fold axis, here the Fab appears to have a preferred orientation, with each of its two hinges sitting on a (partly disordered) EF loop of VP2. (Note that the Fab envelope is a sufficiently low-resolution feature that imposing an icosahedral twofold operation on the Fab density envelope had only a minimal effect on the density shape). The density for the Fab being weaker than that of the capsid can be attributed, at least in part, to the fact that at most 30 copies of the Fab can bind the virion over the 2-fold axis. Both the contour level needed to visualize the Fab and the quality of fit of this density to the Fab model indicated higher occupancy and more structural consistency in this complex than we saw in our other complexes with Mab.

In the r135+m25 icosahedrally averaged map, and in all of the focused classes that were calculated from the r135+m25 image stack, we looked under the bottom surface of the Fab, trying to find density for a peptide connection (perhaps similar to the density connections that we saw in the focus classes of antibody-decorated 80S particles (Fig. 1b)). Instead, the bottom surface of the Fab (above the 2-fold axis) consistently lacked an obvious connection; and the 2-fold hole was occupied by a density that we tentatively identify as the partially retracted C-terminus of VP2

(Fig. 4b). In contrast, in focused classifications centered on the 2-fold axis, including the quasi-3-fold holes, we observed 61% of the asymmetric particles exhibiting a clear density for the N-terminus of VP1 emerging from the quasi 3-fold hole (Fig. 4c), with the GH loop of VP3 in an extended conformation as described in the m135 model (Fig. 2c.).

Visualizing the exposed N-terminal helix of VP1. Interestingly, we observed a focused class for the screening data comprising of 21% of the 966,840 asymmetric units of the virus where the lower half of the Fab contacts both VP2 shoulders, but asymmetrically tilts towards one of the shoulders (Fig. 4d). This causes the top half of the Fab to become less well ordered compared to the lower half of the molecule. In this class, the tilted Fab leans against a long, straight, upward-projecting density feature. The projecting density is unusual in its appearance with one wide dimension and a flat dimension (Fig. 4d).

The observed shape of the density closely matches the shape of an idealized alpha helix built with the sequence of the first 20 residues of VP1 (the amphipathic character of this helix is known to be evolutionarily conserved [11]). The helical density observed in our map (Fig. 4d) appears on the top surface of the VP2 EF loop, in the same location that a difference density peak was previously observed between low-resolution structures of V8 protease treated and untreated 135S particles [31] (Fig. S3b). Similar column-like density features were seen in some of our other focus classes, but the density was never quite as convincing as it was in this example.

Taken together these data suggest that the Fab in r135+m25 particles is bound to a copy of the VP1 N-terminus that has exited at a nearby quasi-3-fold axis, and its location above the 2-fold hole is determined by interactions of the framework region of the Fab and the extreme N-terminal residues of VP1 with the VP2 GH loops.

Receptor-induced 135S particles incubated with mAb at 37˚C

To account for the difference in the binding pattern of the Fab between the m135 and r135+m25 reconstructions, we postulated that lowering the temperature had an effect on the pattern of Fab binding. To that end the experiment was performed in the same manner as the r135+m25 conditions, except that the temperature for incubating with antibody was maintained at 37˚C. The Fab density that was observed (Fig. 5a-b) appeared to be a superposition of the m135 and r135+m25 binding patterns, Thus, the density for the Fab is rod-like (as it was in the m135 reconstruction), but there is also significant density above the 2-fold axis which includes density corresponding to the upper half of the Fab (as was observed in the r135+m25 reconstruction). The reduced occupancy of well-ordered Fab molecules at the 2-fold site (in r135+m37, relative to r135+m25) suggests that the higher temperature of incubation with antibody destabilizes the interaction of Fab with the VP2 GH loop. As was the case in the m135 structure, the r135+m37

reconstruction has readily interpretable density for the VP1 N-terminus exiting at the quasi-3-fold hole. Given that the r135+m37 map appears to be a lower-resolution (see Table S1) superposition of two better-determined structures, and not relevant to biological infection, we elect not to report an atomic model for it.

Possible pentamers of capsid protein VP4.

The small myristoylated capsid protein VP4 [18], is believed to play an important role in the protection of viral RNA (as RNA crosses the gap between virus and membrane) and in the penetration of host cell membranes[38,39]. In 160S virions, prior to capsid expansion, pentamers of poliovirus VP4 lie flat on the inner surface of the capsid, cupping the VP3 beta tube in a ring of five myristates [9,18] (Fig. 6, leftmost panel). The N-terminal residues (1-45) of VP4 intertwine in a pinwheel arrangement to form a 60Å diameter disk, while the C-terminal residues (46-70) extend away from the disk, towards the 3-fold axes, in a 5-pointed star arrangement [2]. In contrast, in 80S empty capsids, most if not all of the RNA is gone and there is no density for VP4 [25,26] (Fig. 6, rightmost panel). But what happens to VP4 in between those initial and final states?

Our five high-resolution structures of 135S-like particles offer some intriguing indications that many of the VP4 pentamers may, indeed, remain intact within the virus capsid, with their distances from the protein shell increasing as the capsid shifts outward. Like many other 135S-like expanded picornavirus structures, our

maps show a distinct 10Å-thick layer on the outer surface of the unstructured RNA density (top row center of Fig. 1a, and Fig. 3a right). Although this layer has commonly been attributed to RNA [29,32], we believe that its shape and dimensions are consistent with VP4 (see below).

In "early 135S particles" (i.e. expanded but with the VP1 N-terminus mostly inside), as seen in the "r135" and "h135" structures, the putative VP4 density is consistently cup-shaped in profile (Fig. 6 second panel from left). Seen face-on, the density feature has a radial position and a diameter similar to that of a native VP4 pentamer. Like VP4 pentamers, the density feature is around 10Å thick (which is much too thin to be duplex RNA). As in native virus, the center of the cup (near the 5-fold axis) contacts the VP3 beta tube; but further from the 5-fold axis, unlike native virus, the density is seen to curve away from the capsid (as if it were peeling off of the inner surface of the capsid). Notably, the shape of the density is pentagonal, with a large central hole, which differs from the star-shaped density of the native pentamer. This would require some concerted conformational change to occur as the pentamer detached.

In the "late 135S particles" (expanded, with the VP1 N-terminus mostly externalized), as seen in the m135, r135+m25 and r135+m37 data sets, the cup-shaped density feature is slightly flatter, and is positioned slightly further away from the inner capsid surface (at ~14Å) (Fig. 6, third panels from left).

These results are consistent with claims from published literature (15, 40) in which VP4 was detected biochemically in preparations of 135S particles. Moreover, because VP4 plays a key role in viral infection [40], at least some VP4 must remain present in 135S particles to explain the observation that these particles remain infectious [15,16]. Therefore, we conclude that the thin layer immediately adjacent to the capsid that has previously been attributed to RNA is more likely to be residual VP4 that is not externalized until the RNA genome is released.

Discussion.

Picornavirus cell-entry is still an area of active research. In the present study we have gained further insight into the dynamics of the expanded genome-containing infectious intermediate of poliovirus, which is known as the 135S particle. Importantly, we show that the 135S particle, which was thought to be a unique structure, is instead an ensemble of structures, that expansion is not completely coupled to externalization the N-terminal extension of VP1 as previously thought, and that a significant fraction of VP4 remains in partially occupied but well-ordered structures on the inner surface of the particle.

Decoupling expansion and externalization of the VP1 N-terminus – One of the unexpected findings of the current study was the observation of 135S particles which were expanded but had not externalized the VP1 N-terminus. Thus in the r135 and h135 structures, where the 135S particles had been prepared by

445 protocols that were believed to result in both expansion and externalization of the
446 VP1 N-terminus, icosahedrally averaged maps showed that the VP3 GH loop was
447 in a conformation that blocked the hole at the quasi-3-fold axes and there was no
448 detectable density for the VP1 N-terminus. This observation contrasts with
449 biochemical studies that show that the VP1 N-terminus was accessible to
450 proteases and to antibodies and with earlier structural studies of 135S particles of
451 poliovirus and other enteroviruses. Indeed, we observed weak but significant
452 density for the externalized VP1 N-terminus in a recent intermediate resolution
453 (5.5Å) structure of the 135S particles that were prepared by the same heating
454 protocol [30]. To address this apparent discrepancy, we tried applying our current
455 cryoEM software protocols for classification and data processing to the older lower-
456 resolution data set and produced a fenestrated reconstruction that lacked
457 significant density for the VP1 N-terminus (data not shown). We conclude that the
458 samples that produced both structures contained a mixture of structures and that
459 the methods used to select particles to be included in the earlier lower-resolution
460 reconstruction resulted in enrichment in a minority population of particles with the
461 VP1 N-terminus exposed.
462
463 **Where does the VP1 N-terminus exit the virion -** Previous structural and
464 biochemical characterization of the 135S particle of poliovirus (and other related
465 picornaviruses) using cryoEM, crystallography, and antibody studies, led to a
466 model wherein, upon expansion, the N-terminus of VP1 initially exits via the 2-fold
467 hole, and later gets locked into the quasi-3-fold channel through a “gear-shift”

motion[17,24,27,30]. However, in none of our recent panel of structures did we observe evidence for such a motion. Instead, the density for the N-terminus of VP1 in 135S particles, whenever it was externalized and trapped by an antibody, was consistently observed to occupy the quasi-3-fold channel. Although we cannot rule out a model in which VP1 transiently exits via a hole at the 2-fold axis during the dynamic process of externalization, our recent maps suggest that any such externalized polypeptide is either quickly re-internalized, or quickly migrates to the quasi-3-fold axis. It is also worth noting that even after a long incubation with the monoclonal antibody (m135, r135+m25, and r135+m37), in all cases densities for the VP1 N-terminal extension and for the antibody were consistently weaker than capsid, which suggests that some VP1 N-termini may remain inside the capsid.

A revised model for the virus-to-135S transition. Taken together our current results suggest a process with three major steps. First, upon binding to the receptor at 37°C or exposure to high temperature (50°C) the virus expands and a significant fraction of VP4 is externalized. This step is concomitant with the loss "pocket factor" and of internal and external stabilizing interactions among neighboring protomers through their N- and C-termini and loops on the outer surface. In a second step, the residues in the VP1 N-terminus are then reorganized such that residues 69-64 run up through the quasi-3-fold. It is clear that this second step must happen during infection because biochemical studies show that the VP1 N-terminus is inserted into membranes in *in vitro* models [11,19] and during infection, and plays a key role in the late stages of viral entry [41]. We would argue,

however, that the externalization of the VP1 N-terminus is transient and reversible on the time scales relevant to infection (minutes) and that exposure of a significant fraction of the VP1 N-termini on this time scale requires the presence of a trap. Trapping agents could include cellular membranes during infection [11,15], liposomes in *in vitro* model systems [11,19,20], or antibodies that bind the VP1 N-terminus once exposed [22,24]. In order to explain the observation of stable structures in which the VP1 N-terminus is clearly externalized, we postulate a third step in which the VP1 N-terminus slowly becomes locked on the outside of the capsid even in the absence of trapping agents, perhaps by forming stable interactions with the GH loops of VP3 and VP1, as seen in the m135 structure, in our previous intermediate-resolution reconstruction of the poliovirus 135S particle[30], and in the structures of the 135S particles of other enteroviruses [17,29,42]. What proportion of the N-termini are exposed in 135S particles, during natural infections, in the presence of cellular membranes, is now an open question.

Wither the VP1 N-terminus after leaving the capsid. Although it is clear that residues 69-64 of the VP1 N-terminus exit the capsid at the quasi-3-fold, the course of the externalized residues 1-61 that are distal to the exit point is less clear. In all of our structures, residues 61-56 are disordered. Based on where Fab density is seen, residues 55-42 (which constitute the antibody binding site) can be located either above a 2-fold axis (r135+m25), or above a quasi-3-fold axis (m135), or both (r135+m37). Finally, the results from an earlier low-resolution structure of the 135S particles [31] and the clear density

amphipathic helix of VP1 in the r135+m25 structure reported here demonstrates that a significant fraction of the first 20 amino acids of VP1 can bind at the top of the EF loop of VP2. These results are summarized in Fig. 7.

Significance of the amphipathic helix of VP1. Earlier studies from our group[11,19] demonstrated the externalization of the VP1 N-terminus and described its role in the binding of 135S particles to membranes. Using floatation assays and V8-protease-based cleavage of the 135S particles, the membrane-interacting part of the peptide was localized to the first 30 amino acids in the sequence[11,19]. Further analysis predicted that the first 20 amino acids would adopt a helical conformation[11], with the helix having a hydrophobic and a hydrophilic side (a common membrane-interactive structural motif). Subsequently, single particle cryoEM analysis of V8-cleaved and uncleaved 135S particles[36] suggested that the externalized VP1 N-terminus would sometimes be anchored on top of the VP2 EF-loop. However, the density for the amphipathic helix had never been visualized directly. In the present study, we were fortunate to be able to visualize clear density for the entire helix, and to confirm that the helix is located in the same location that the V8-cleavage difference density from an earlier study [31] had predicted it to be (Fig. 4d, Fig. S3b). The fact that the helix is only clearly visible in focused reconstructions from the screening data set suggests that the interactions between the helix and the VP2 may be weak. However, we speculate that, even if the localization of the helix at the tip of the VP2 EF loop is transient at physiological temperature, by increasing the number of copies of the N-termini at

a higher elevation on the virus particle, this interaction may drive the association with membrane, may facilitate engulfment of the virus particle at the cell surface and internalization into endosomes [43], and may serve as an asymmetric trigger for the translocation of the genome into the cytosol [20]

Difference in antibody density under different conditions. Another puzzling aspect of the structures presented here is the observation that the Fab in the complexes produced by incubating with PVR at 37˚C then with antibody at 25 ˚C binds above the 2-fold hole, whereas the complexes produced during higher-temperature incubations showed Fab density above the quasi-3-fold axes. A likely explanation for our observations is that some of the N-termini of VP1 become externalized via the quasi-3-fold hole during the initial 3-min. incubation with receptor at 37˚C, and their N-terminal helices find the binding site on the VP2 EF loop, where they remain trapped once the temperature is lowered to 25˚C. Upon subsequent incubation with antibody at room temperature, this configuration is further stabilized by nonspecific contacts between the antibody, the VP1 N-terminal helix, and the VP2 EF loops. In the maps (Fig. 4a-b), this binding mode manifests as a well-ordered density that recognizably corresponds to both halves of the Fab portion of the antibody.

In contrast, when the particles are maintained at 37˚C or 39˚C during antibody binding, the higher temperature reduces the stability of the specific interactions of the VP1 N-terminal helix with the VP2 EF loop, the nonspecific interactions of the

560 hinges of the Fab with the VP2 EF loop “shoulders”; and the nonspecific
561 interactions of the VP1 helix with the sides of the Fab. Thus, the 2-fold binding of
562 Fab was reduced at 37 ˚C, and almost eliminated at 39˚C. Instead, a greater
563 proportion of the Fab moieties were bound closer to the quasi-3-fold hole, where
564 Fab orientations were less well-constrained, and the Fab density was
565 consequently more diffuse.
566
567 **Presence of VP4 in an expanded particle**. VP4 is a myristoylated, pore-forming
568 protein that is implicated in the translocation the RNA genome across
569 membranes[18,38,40]. This protein was thought to be completely lost after
570 conversion to the 135S state[11-13]. However, biochemical and infectivity assays
571 indicate that at least 25% of VP4 remains associated with the virus particle, and
572 that the 135S particle remains infectious[15,44] (Fig. 6b and Fig. S2). In several
573 related picornaviruses, reports of expanded virus structures have noted the
574 disappearance of VP4 from the inner surface of the capsid, and have attributed all
575 of the unstructured density inside of the capsid to RNA, including a thin 10Å-thick
576 layer at the periphery of the icosahedrally-averaged "RNA ball"[29,32]. However,
577 in our panel of expanded genome-containing structures, we can alternatively
578 account for the density under the 5-fold peak using a native atomic model of the
579 VP4 pentamer (Fig. 6). Moreover, an unmistakable gradual curving of the VP4
580 layer away from the capsid, peeling off of the inner surface, was seen in the r135
581 and h135 structures (Fig. 6.) that is remarkably similar in appearance to the density
582 that has been ascribed to RNA in previous studies with other enteroviruses[29,32]

583 . VP4 has the capacity to bind to RNA[45] and perhaps that is the reason it is being
584 held in place (at its original radius in native virus) while the rest of the capsid
585 expands radially. Nevertheless, it remains unclear how VP4, thus separated from
586 the capsid, possibly still associated with RNA, and with pentamers intact or not,
587 manages to exit the capsid and to embed itself in the membrane. This will be an
588 important avenue to explore in understanding the crucial genome-translocation
589 step in picornavirus infection.
590
591 **Materials and Methods**
592
593 **Virus and antibody.**
594 Poliovirus type 1 Mahoney strain was purified by infecting Hela S3 suspension
595 cells at an MOI=10 for 6hrs at 37˚C. Infected cells were spun down, washed with
596 phosphate buffered saline (PBS:137 mM NaCl, 2.7 mM KCl, 1.1 mM KH_2PO_4, 6.5
597 mM Na_2HPO_4, 0.7 mM $CaCl_2$, 0.5 mM $MgCl_2$) and frozen at -80˚C. Virus was
598 released from the cells by repeated freeze-thawing of the infected cell pellet in
599 RSB buffer (10mM Tris pH 7.3, 10 mM NaCl, 1.5 mM $MgCl_2$, 1% IGEPAL CA-630)
600 and clarification of the cell debris through centrifugation. The virus was pelleted
601 through ultracentrifugation and layered on a CsCl density gradient. Subsequently,
602 the virus band was collected and dialysed against PBS before being flash frozen
603 in liquid nitrogen and stored at -80˚C.
604

The anti-VP1 monoclonal antibody (one of two monoclonal antibodies in a pan-Enterovirus ELISA detection kit) was obtained from Quidel (Athens, Ohio).

Plaque Assay

Vero cells were grown in 6-well plates until confluency at 37˚C and 5% CO_2. The cells were then infected with serial dilutions of poliovirus. At 36 h post-infection cells were fixed with 10% formaldehyde and stained with 0.1% crystal violet.

In vitro generation of poliovirus 135S and 135S-like particles

Anti-VP1 antibody triggered 135S-like particles were generated by mixing 18µL of virus suspension (0.4mg/ml) with 3µL of anti-VP1 antibody (3.2mg/ml) and incubated for 1.5 h at 39˚C in a thermal cycler. To generate 135S particles, PV suspension was first buffer exchanged into a low salt buffer (20mM Tris-Cl pH 7.5, 2mM $MgCl_2$). The receptor-triggered conversion of PV was induced by mixing 18.6µL of PV (0.5mg/ml) with 0.4µL of PVR/CD155 (6.1mg/ml) on ice before incubating at 37˚C for 3 min. The reaction was quenched on ice. Heat-triggered 135S particles were generated by heating native PV (in the low salt buffer) to 50˚C for 3 minutes, before quenching the reaction on ice. The r135+m25/37 particles were produced by incubating PV with PVR, as described above, followed by the addition of the anti-VP1 mAb (150x molar excess over virus) and incubation at 25˚C or 37˚C for 1 h.

Cryo-Electron Microscopy and data collection

Carbon-backed lacey grids (Ted Pella) were glow discharged in an easiGLO (PELCO, Fresno, California) glow discharge unit by applying a current of 15mA for 30s. To the freshly glow-discharged grids, 3.0-3.5µL of virus or virus-ligand mixture was applied. The samples were then allowed to adsorb on the grid for 30s before blotting away the excess buffer using a blot force of 6 and blot time of 6s in a FEI Vitrobot Mark IV (ThermoFisher). The grids were plunge frozen in a liquid ethane slush and stored in liquid nitrogen until imaging. Data collection parameters are listed in Table S1.

Image processing

Image processing of micrographs was performed within Relion 3.0 [46]. Individual movie frames were aligned and dose-weighted with the Relion implementation of motion correction by applying a negative B-factor of -150 [47]. CTF parameter estimation was performed using Gctf v1.06 [48] on dose-weighted micrographs. Particle-picking was performed in crYOLO[49] by training the neural network on an initial subset of ~300 manually picked particles from several micrographs sampling a range of defocus values. Subsequently, the particle picker was deployed on the complete dataset to identify and save particle co-ordinates which were then imported into Relion. The picked particles were extracted, binned by 4 and subjected to a single round of 2D classification and obviously junk classes were discarded prior to 3D classification. The particle stack was refined against a representative class obtained at the end of the 3D classification. After the first round of refinement, the dataset was subjected to CTF refinement [46] by

651 estimating beam tilt, per-particle defocus and astigmatism followed by Bayesian
652 polishing [46] with default parameters. Icosahedral symmetry was imposed in
653 every round of refinement and the reference model was filtered to 60Å to prevent
654 model bias. The final resolution (0.143 gold standard FSC) of the structures (Table
655 S1) was obtained through the Postprocessing job type in Relion, where a density-
656 based mask enclosing the capsid was applied to estimate the FSC between two
657 independently processed half datasets. Local resolution estimates were also
658 obtained by running the Relion's implementation of local resolution algorithm.
659
660 **Asymmetric focused classes**
661 After assignment of icosahedral orientations to the particle images, a cylindrical
662 mask was prepared using SPIDER[50] with a diameter of 105Å, centered on the
663 viral 2-fold and enclosing two copies of the quasi 3-fold axis. The initial height of
664 475Å was then limited to a spherical shell by applying minimum cutoff at 154Å.
665 Then, using relion_particle_symmetry_expand a new STAR file containing 60
666 icosahedrally related orientations for each particle in the stack was generated. This
667 symmetry expanded stack was then subjected to a masked 3D classification
668 routine in which orientational and translational searches were disabled, the T-value
669 was set to 40, and 5 density classes were generated.
670
671 **Model building and refinement**
672 A starting model for m135 was assembled from 1HXS and previously published
673 high-resolution structures of the expanded poliovirus structures [25,51] were

674 docked into the density using COOT [52]. Where none of the pre-existing models
675 for the density fit well, the segments were constructed *de novo*.
676 Models were iteratively built and refined in REFMAC5 and/or phenix_refine and/or
677 phenix_real_space_refine, until no further improvement was possible [53-55]. To
678 avoid model bias, the Fourier transforms of the experimental maps (both
679 amplitudes and phases) were used as refinement standards. The model included
680 a central protomer (VP1, VP2, and VP3) and neighboring proteins related by
681 icosahedral symmetry. Strong restraints were included for stereochemistry,
682 symmetry, and temperature factors.
683

684 **Data Availability**

685 Cryo-EM maps and masks for m135, r135, h135, r135+m25 and r135+m37
686 conditions are deposited in the EMDB with accession codes EMD- 20275, EMD-
687 20276, EMD-20469, EMD-20546 and EMD-20474 respectively. Atomic co-
688 ordinates for all the maps except r135+m37 can be accessed from the PDB with
689 the following codes 6P9O (m135), 6P9W (r135), 6PSZ (h135), 6Q0B (r135+m25).
690

691 **Figure preparation**

692 Figures and illustrations were prepared using PyMol (Schrödinger, LLC), Chimera
693 [56], ChimeraX [57] sourced through the SBGrid Consortium[58] and compiled in
694 Adobe Illustrator (Adobe, USA)
695

696 **Acknowledgements.**
697 We would like to thank Drs. Lawrence Shapiro and Oliver Harrison (Columbia
698 University) for providing us with PVR, Sara McCoy (Quidel) for providing the anti

VP1 antibody, Dr. David Bhella (University of Glasgow) and Dr. Simon Jenni (Harvard University) for helping us run the asymmetric focused classification. We would also like to thank members of the SBGrid team for maintaining the computing environment. Dr. Takanori Nakane (MRC-LMB) is acknowledged for sharing the code to plot the resolution distribution in 3D volumes. We would like to acknowledge the Astbury Biostructure Laboratory (ABSL) for Titan Krios cryo-EM data collection which was funded by the University of Leeds and the Wellcome Trust (108466/Z/15/Z) as well as the Harvard Cryo-EM Center for Structural Biology This study was supported by an NIH grant (AI020566) to J.M.H.

Author Contributions.

Conceived and designed the experiments: JMH, MS, DJF, PNMS, KK. Performed the experiments: PNMS, KK, EH, EG. Analysed the data: PNMS, DJF, JMH. Wrote the paper: DJF, PNMS, JMH, MS.

References

1. Ryu W-S. Chapter 11 - Picornavirus. In: Ryu W-S, editor. Molecular Virology of Human Pathogenic Viruses. Boston: Academic Press; 2017. pp. 153–164. doi:https://doi.org/10.1016/B978-0-12-800838-6.00011-4

2. Hogle JM, Chow M, Filman DJ. Three-dimensional structure of poliovirus at 2.9 A resolution. Science 229:1358-1365.

3. Ayers T, Lopez A, Lee A, Kambhampati A, Nix WA, Henderson E, et al. Acute Flaccid Myelitis in the United States: 2015-2017. Pediatrics. 2019;144: e20191619. doi:10.1542/peds.2019-1619

4. Sejvar JJ, Lopez AS, Cortese MM, Leshem E, Pastula DM, Miller L, et al. Acute Flaccid Myelitis in the United States, August-December 2014: Results of Nationwide Surveillance. Clin Infect Dis. 2016;63: 737–745. doi:10.1093/cid/ciw372

5. Mendelsohn CL, Wimmer E, Racaniello VR. Cellular receptor for poliovirus: molecular cloning, nucleotide sequence, and expression of a new member of the immunoglobulin superfamily. Cell. 1989;56: 855–865. doi:10.1016/0092-8674(89)90690-9

6. Takai Y, Irie K, Shimizu K, Sakisaka T, Ikeda W. Nectins and nectin-like molecules: roles in cell adhesion, migration, and polarization. Cancer Sci. John Wiley & Sons, Ltd (10.1111); 2003;94: 655–667. doi:10.1111/j.1349-7006.2003.tb01499.x

7. Strauss M, Filman DJ, Belnap DM, Cheng N, Noel RT, Hogle JM. Nectin-like interactions between poliovirus and its receptor trigger conformational changes associated with cell entry. Kirkegaard K, editor. Journal of Virology. American Society for Microbiology; 2015;89: 4143–4157. doi:10.1128/JVI.03101-14

8. Tsang SK, Danthi P, Chow M, Hogle JM. Stabilization of poliovirus by capsid-binding antiviral drugs is due to entropic effects. J Mol Biol. 2000;296: 335–340. doi:10.1006/jmbi.1999.3483

9. Filman DJ, Syed R, Chow M, Macadam AJ, Minor PD, Hogle JM. Structural factors that control conformational transitions and serotype specificity in type 3 poliovirus. The EMBO Journal. John Wiley & Sons, Ltd; 1989;8: 1567–1579. doi:10.1002/j.1460-2075.1989.tb03541.x

10. Belnap DM, Filman DJ, Trus BL, Cheng N, Booy FP, Conway JF, et al. Molecular tectonic model of virus structural transitions: the putative cell entry states of poliovirus. Journal of Virology. American Society for Microbiology; 2000;74: 1342–1354. doi:10.1128/JVI.74.3.1342-1354.2000

11. Fricks CE, Hogle JM. Cell-induced conformational change in poliovirus: externalization of the amino terminus of VP1 is responsible for liposome binding. Journal of Virology. American Society for Microbiology; 1990;64: 1934–1945.

12. de Sena J, Mandel B. Studies on the in vitro uncoating of poliovirus II. Characteristics of the membrane-modified particle. Virology. Academic Press; 1977;78: 554–566. doi:10.1016/0042-6822(77)90130-1

13. Fenwick ML, Cooper PD. Early interactions between poliovirus and ERK cells: Some observations on the nature and significance of the rejected particles. Virology. Academic Press; 1962;18: 212–223. doi:10.1016/0042-6822(62)90007-7

14. Butan C, Filman DJ, Hogle JM. Cryo-Electron Microscopy Reconstruction Shows Poliovirus 135S Particles Poised for Membrane Interaction and RNA Release. Journal of Virology. American Society for Microbiology Journals; 2014;88: 1758–1770. doi:10.1128/JVI.01949-13

15. Curry S, Chow M, Hogle JM. The poliovirus 135S particle is infectious. Journal of Virology. American Society for Microbiology Journals; 1996;70: 7125–7131.

16. Huang Y, Hogle JM, Chow M. Is the 135S Poliovirus Particle an Intermediate during Cell Entry? Journal of Virology. American Society for Microbiology Journals; 2000;74: 8757–8761. doi:10.1128/JVI.74.18.8757-8761.2000

17. Ren J, Wang X, Hu Z, Gao Q, Sun Y, Li X, et al. Picornavirus uncoating intermediate captured in atomic detail. Nature Communications. 2013;4: 1929. doi:10.1038/ncomms2889

18. Chow M, Newman JFE, Filman D, Hogle JM, Rowlands DJ, Brown F. Myristylation of picornavirus capsid protein VP4 and its structural significance. Nature. Nature Publishing Group; 1987;327: 482–486. doi:10.1038/327482a0

19. Tuthill TJ, Bubeck D, Rowlands DJ, Hogle JM. Characterization of Early Steps in the Poliovirus Infection Process: Receptor-Decorated Liposomes Induce Conversion of the Virus to Membrane-Anchored Entry-Intermediate Particles. Journal of Virology. American Society for Microbiology Journals; 2006;80: 172–180. doi:10.1128/JVI.80.1.172-180.2006

20. Strauss M, Levy HC, Bostina M, Filman DJ, Hogle JM. RNA transfer from poliovirus 135S particles across membranes is mediated by long umbilical connectors. Journal of Virology. American Society for Microbiology; 2013;87: 3903–3914. doi:10.1128/JVI.03209-12

21. Groppelli E, Levy HC, Sun E, Strauss M, Nicol C, Gold S, et al. Picornavirus RNA is protected from cleavage by ribonuclease during virion uncoating and transfer across cellular and model membranes. Sarnow P, editor. PLoS Pathog. Public Library of Science; 2017;13: e1006197. doi:10.1371/journal.ppat.1006197

22. Li Q, Yafal AG, Lee YM, Hogle J, Chow M. Poliovirus neutralization by antibodies to internal epitopes of VP4 and VP1 results from reversible exposure of these sequences at physiological temperature. Journal of Virology. American Society for Microbiology; 1994;68: 3965–3970.

23. Roivainen M, Piirainen L, Rysä T, Närvänen A, Hovi T. An immunodominant N-terminal region of VP1 protein of poliovirion that is buried in crystal structure can be exposed in solution. Virology. 1993;195: 762–765.

24. Lin J, Lee LY, Roivainen M, Filman DJ, Hogle JM, Belnap DM. Structure of the Fab-labeled “breathing” state of native poliovirus. Journal of Virology. American Society for Microbiology; 2012;86: 5959–5962. doi:10.1128/JVI.05990-11

25. Strauss M, Schotte L, Karunatilaka KS, Filman DJ, Hogle JM. Cryo-electron Microscopy Structures of Expanded Poliovirus with VHHs Sample the Conformational Repertoire of the Expanded State. Dermody TS, editor. Journal of Virology. American Society for Microbiology Journals; 2017;91: e01443–16. doi:10.1128/JVI.01443-16

26. Levy HC, Bostina M, Filman DJ, Hogle JM. Catching a virus in the act of RNA release: a novel poliovirus uncoating intermediate characterized by cryo-electron microscopy. Journal of Virology. American Society for Microbiology; 2010;84: 4426–4441. doi:10.1128/JVI.02393-09

27. Lin J, Cheng N, Chow M, Filman DJ, Steven AC, Hogle JM, et al. An externalized polypeptide partitions between two distinct sites on genome-released poliovirus particles. Journal of Virology. American Society for Microbiology; 2011;85: 9974–9983. doi:10.1128/JVI.05013-11

28. Shingler KL, Yoder JL, Carnegie MS, Ashley RE, Makhov AM, Conway JF, et al. The enterovirus 71 A-particle forms a gateway to allow genome release: a cryoEM study of picornavirus uncoating. Rey FA, editor. PLoS Pathog. 2013;9: e1003240. doi:10.1371/journal.ppat.1003240

29. Zhu L, Sun Y, Fan J, Zhu B, Cao L, Gao Q, et al. Structures of Coxsackievirus A10 unveil the molecular mechanisms of receptor binding and viral uncoating. Nature Communications. Nature Publishing Group; 2018;9: 4985. doi:10.1038/s41467-018-07531-0

30. Butan C, Filman DJ, Hogle JM. Cryo-electron microscopy reconstruction shows poliovirus 135S particles poised for membrane interaction and RNA release. Journal of Virology. American Society for Microbiology; 2014;88: 1758–1770. doi:10.1128/JVI.01949-13

31. Bubeck D, Filman DJ, Cheng N, Steven AC, Hogle JM, Belnap DM. The structure of the poliovirus 135S cell entry intermediate at 10-angstrom resolution reveals the location of an externalized polypeptide that binds to membranes. Journal of Virology. American Society for Microbiology; 2005;79: 7745–7755. doi:10.1128/JVI.79.12.7745-7755.2005

32. Organtini LJ, Makhov AM, Conway JF, Hafenstein S, Carson SD. Kinetic and structural analysis of coxsackievirus B3 receptor interactions and formation of the A-particle. Journal of Virology. 2014;88: 5755–5765. doi:10.1128/JVI.00299-14

33. Kaplan G, Freistadt MS, Racaniello VR. Neutralization of poliovirus by cell receptors expressed in insect cells. Journal of Virology. American Society for Microbiology (ASM); 1990;64: 4697–4702.

34. Gómez Yafal AG, Kaplan G, Racaniello VR, Hogle JM. Characterization of poliovirus conformational alteration mediated by soluble cell receptors. Virology. 1993;197: 501–505. doi:10.1006/viro.1993.1621

35. Wetz K, Kucinski T. Influence of different ionic and pH environments on structural alterations of poliovirus and their possible relation to virus uncoating. Journal of General Virology. Microbiology Society; 1991;72: 2541–2544. doi:10.1099/0022-1317-72-10-2541

854 36. Bubeck D, Filman DJ, Hogle JM. Cryo-electron microscopy reconstruction
855 of a poliovirus-receptor-membrane complex. Nature Structural & Molecular
856 Biology. Nature Publishing Group; 2005;12: 615–618.
857 doi:10.1038/nsmb955

858 37. Tsang SK, McDermott BM, Racaniello VR, Hogle JM. Kinetic analysis of
859 the effect of poliovirus receptor on viral uncoating: the receptor as a
860 catalyst. Journal of Virology. American Society for Microbiology Journals;
861 2001;75: 4984–4989. doi:10.1128/JVI.75.11.4984-4989.2001

862 38. Panjwani A, Strauss M, Gold S, Wenham H, Jackson T, Chou JJ, et al.
863 Capsid protein VP4 of human rhinovirus induces membrane permeability
864 by the formation of a size-selective multimeric pore. Rey FA, editor. PLoS
865 Pathog. Public Library of Science; 2014;10: e1004294.
866 doi:10.1371/journal.ppat.1004294

867 39. Tosteson MT, Chow M. Characterization of the ion channels formed by
868 poliovirus in planar lipid membranes. Journal of Virology. American Society
869 for Microbiology; 1997;71: 507–511.

870 40. Danthi P, Tosteson M, Li Q-H, Chow M. Genome Delivery and Ion Channel
871 Properties Are Altered in VP4 Mutants of Poliovirus. Journal of Virology.
872 American Society for Microbiology Journals; 2003;77: 5266–5274.
873 doi:10.1128/JVI.77.9.5266-5274.2003

874 41. Kirkegaard K. Mutations in Vp1 of Poliovirus Specifically Affect Both
875 Encapsidation and Release of Viral RNA. Journal of Virology. American
876 Society for Microbiology (ASM); 1990;64: 195–206.

877 42. Xu L, Zheng Q, Li S, He M, Wu Y, Li Y, et al. Atomic structures of
878 Coxsackievirus A6 and its complex with a neutralizing antibody. Nature
879 Communications. Nature Publishing Group; 2017;8: 505.
880 doi:10.1038/s41467-017-00477-9

881 43. Brandenburg B, Lee LY, Lakadamyali M, Rust MJ, Zhuang X, Hogle JM.
882 Imaging Poliovirus Entry in Live Cells. Sugden B, editor. Plos Biol. Public
883 Library of Science; 2007;5: e183. doi:10.1371/journal.pbio.0050183

884 44. Lyu K, Ding J, Han J-F, Zhang Y, Wu X-Y, He Y-L, et al. Human
885 enterovirus 71 uncoating captured at atomic resolution. Hutt-Fletcher L,
886 editor. Journal of Virology. 5 ed. American Society for Microbiology
887 Journals; 2014;88: 3114–3126. doi:10.1128/JVI.03029-13

888 45. McGregor S, Mayor HD. Biophysical and Biochemical Studies on
889 Rhinovirus and Poliovirus II. Chemical and Hydrodynamic Analysis of the
890 Rhinovirion. Journal of Virology. American Society for Microbiology
891 Journals; 1971;7: 41–46. doi:10.1146/annurev-biophys-062215-010822

892 46. Zivanov J, Nakane T, Forsberg BO, Kimanius D, Hagen WJ, Lindahl E, et
893 al. New tools for automated high-resolution cryo-EM structure
894 determination in RELION-3. eLife Sciences. 2018;7: 163.
895 doi:10.7554/eLife.42166

896 47. Zivanov J, Nakane T, Scheres SHW. A Bayesian approach to beam-
897 induced motion correction in cryo-EM single-particle analysis. IUCrJ.
898 2019;6: 5–17. doi:10.1107/S205225251801463X

899 48. Zhang K. Gctf: Real-time CTF determination and correction. Journal of
900 Structural Biology. 2016;193: 1–12. doi:10.1016/j.jsb.2015.11.003

901 49. Wagner T, Merino F, Stabrin M, Moriya T, Antoni C, Apelbaum A, et al.
902 SPHIRE-crYOLO is a fast and accurate fully automated particle picker for
903 cryo-EM. Commun Biol. 2019;2: 218. doi:10.1038/s42003-019-0437-z

904 50. Frank J, Radermacher M, Penczek P, Zhu J, Li Y, Ladjadj M, et al.
905 SPIDER and WEB: processing and visualization of images in 3D electron
906 microscopy and related fields. Journal of Structural Biology. 1996;116:
907 190–199. doi:10.1006/jsbi.1996.0030

908 51. Strauss M, Schotte L, Thys B, Filman DJ, Hogle JM. Five of Five VHHs
909 Neutralizing Poliovirus Bind the Receptor-Binding Site. Dermody TS,
910 editor. Journal of Virology. American Society for Microbiology; 2016;90:
911 3496–3505. doi:10.1128/JVI.03017-15

912 52. Emsley P, Cowtan K. Coot: model-building tools for molecular graphics.
913 Acta Crystallogr Sect D Biol Crystallogr. International Union of
914 Crystallography; 2004;60: 2126–2132. doi:10.1107/S0907444904019158

915 53. Murshudov GN, Vagin AA, Dodson EJ. Refinement of macromolecular
916 structures by the maximum-likelihood method. Acta Crystallogr Sect D Biol
917 Crystallogr. International Union of Crystallography; 1997;53: 240–255.
918 doi:10.1107/S0907444996012255

919 54. Afonine PV, Poon BK, Read RJ, Sobolev OV, Terwilliger TC, Urzhumtsev
920 A, et al. Real-space refinement in PHENIX for cryo-EM and
921 crystallography. Acta Crystallogr D Struct Biol. International Union of
922 Crystallography; 2018;74: 531–544. doi:10.1107/S2059798318006551

923 55. Adams PD, Afonine PV, Bunkóczi G, Chen VB, Davis IW, Echols N, et al.
924 PHENIX: a comprehensive Python-based system for macromolecular
925 structure solution. Acta Crystallogr Sect D Biol Crystallogr. International
926 Union of Crystallography; 2010;66: 213–221.
927 doi:10.1107/S0907444909052925

928 56. Pettersen EF, Goddard TD, Huang CC, Couch GS, Greenblatt DM, Meng
929 EC, et al. UCSF Chimera?A visualization system for exploratory research

and analysis. J Comput Chem. 2004;25: 1605–1612. doi:10.1002/jcc.20084

57. Goddard TD, Huang CC, Meng EC, Pettersen EF, Couch GS, Morris JH, et al. UCSF ChimeraX: Meeting modern challenges in visualization and analysis. Protein Science. 2018;27: 14–25. doi:10.1002/pro.3235

58. Morin A, Eisenbraun B, Key J, Sanschagrin PC, Timony MA, Ottaviano M, et al. Collaboration gets the most out of software. eLife Sciences. eLife Sciences Publications Limited; 2013;2: e01456. doi:10.7554/eLife.01456

Figure Legends

Figure 1: **Anti-VP1 antibody trapped expanded particle** (a.) Top row: The 3D classes from the dataset, with undecorated 160S particles (left), the anti-VP1 mAb decorated 135S-like particle (middle, orange border) and the mAb decorated empty particle (right, yellow border). Second row: Radially colored isosurface representations of the refined particles are shown at a high contour, where the holes at the 2-fold are clearly observed. Third row, isosurface representations of the mAb-decorated 135S (center) and 80S particles (right) contoured at a lower level showing the diffuse density attributable to the bottom half of the Fab part of the mAb. (b) Density for an asymmetric focus class calculated from the mAb decorated 80S particle is depicted in the context of the 2-fold related VP2 subunits (yellow) and a model of a Fab (pink). The tube-like density for the N-terminus of VP1 (arrow) is seen above one of the two 2-fold related VP2 helices.

Figure 2: **Anti-VP1 antibody trapped genome containing particle (m135) is similar to the canonical 135S particle.** (a.) Cage density depiction of the mAb-decorated m135 structure in the vicinity of the 2-fold axes showing the rod shaped density for the lower half of the Fab portion of the mAb and the better ordered density for the capsid proteins of the virus (b.) The canonical poliovirus protomer consisting of VP1 (blue), VP2 (yellow) and VP3 (red) is shown juxtaposed with 5-fold related copies of VP1(cyan) and VP2 (gold). The cyan, gold, and red copies together form the “5-3-3 triangle” having one 5-fold and two 3-fold symmetry axes at its corners. The quasi 3-fold lies at the center of this triangle. Panels (b) and (c) are viewed from outside the virus. (c.) The N-terminus of VP1 (dark blue) is seen exiting the virus capsid through the quasi 3-fold hole. To accommodate this, the GH loop of VP3 (labeled) becomes rearranged and partially disordered. Panels (d-f) are viewed from inside the virus. (d.) The exiting N-terminus (dark blue) contacts the tip of the VP2 bottom loop (labeled) (e.) The bottom loop of VP2, in m135 (yellow), is rearranged relative to native VP2 (magenta) (f.) In m135, the C-terminus of VP2 (dark yellow) becomes ordered on the capsid inner surface, rather than exiting at the 2-fold, as in native virus (magenta).

Figure 3: Receptor-catalyzed, and heat-triggered 135S particles (r/h135). (a.) Radially colored isosurface rendering of the "early" 135S particle at a high contour (left panel) reveals an opening at the 2-fold axis. The panel on the right is shown at a lower contour level with a clipping plane inserted to highlight the re-organised density inside the capsid. These two panels are based on the r135 map, because the two structures are virtually identical (b.) Close up of the quasi-3-fold region. Density for the GH loop of VP3, overlaid on the model, is very similar in the r135 (blue) and h135 (purple) maps. In this conformation, the GH loop of VP3 plugs the quasi-3-fold hole. (c.) Stereo views compare the GH loops of VP3 from the r135 (red), m135 (salmon), and native (orange) structures. The r135 conformation is more similar to the native conformation, as opposed to the m135 model where the GH loop becomes more extended and forms new beta-sheet interactions with a radially-oriented segment of the VP3 D strand.

Figure 4: **Receptor catalyzed 135S particle incubated with the anti-VP1 antibody at 25˚C (r135+m25).** (a.) Radially colored isosurface rendering of the "late" 135S particle shown at high contour (left) to highlight the hole at the 2-fold axis and at a lower contour (right) to highlight binding of the Fab (pink) relative to the capsid (b.) The interaction between the Fab density and the capsid is better resolved following a focused classification centered around the 2-fold symmetry axis of the capsid. (c.) A focus map from (b.) compared with the m135 model, helps to visualize the N-terminus of VP1 (blue) exiting the capsid from the quasi-3-fold hole. The density in this region is poorly resolved in the icosahedral averaged reconstruction (d.) A focused class obtained from the screening data, using a cylindrical mask centered on the 2-fold axis. This map clearly shows a column of density that accommodates the first 20 amino acids of the N-terminus of VP1 (blue). The helix bound to the top surface of VP2 (yellow) is stabilized in a unique orientation by contacts with the Fab (pink). Clearly, the portions of VP2 that bind the base of the helix must be rearranged, in some unknown way that differs from the native conformation of VP2 that is shown (yellow).

Figure 5: **Receptor catalyzed 135S particle incubated with the anti-VP1 antibody at 37˚C (r135+m37). (a.)** Radially colored isosurface rendering of the "late" 135S particle that is produced after receptor-catalyzed expanded virus is incubated with anti-VP1 antibody at 37˚C for 1h. (a.) The panel on the left is contoured at a higher level to show surface details such as holes at the 2-fold and density in the quasi-3-fold. At a lower contour (right), smeared density due to Fab binding (beige) is apparent. (a. and b.) The Fab density in r135+m37 appears to be a super-position of the rod-shaped Fab density that extends over the quasi-3-fold (as seen in m135) and the 2-fold-centered density (as seen in the r135+m25 reconstruction). (c.) a close-up view of the showing the VP1 N-teminus emerging at quasi-3-fold (compare Figs. 2c and 4c).

Figure 6: **Location of VP4 before and after capsid expansion.** Profile (top panel) and face-on (lower panel) view of VP4 (green) in native, r135, m135 and

empty states. The native orientation and location of VP4 has been preserved to highlight the changes in the density, as the capsid expands. Prior to RNA release, VP4 pentamers, somewhat rearranged, appear to remain at their original radius, on the outer surface of the RNA ball, as the rest of the capsid expands outward.

Figure 7: Schematic of VP1 N-terminal stabilization in the r135+m25 state. Four distinct areas in the N-terminal extension of VP1 (dashed blue curve) can be stabilized by binding to the Fab (pink) and the viral capsid (grey). This overall binding pattern is suggested by (i) the observation of residues 70-62 in the m135 complex; (ii) the expectation that amino acids from the 55-42 range (the epitope for the anti-VP1 Ab) will bind to the underside of the anti-peptide mAb; (iii) the anchoring of the N-terminal helix (around residue 21) to the top surface of VP2; and (iv) the nonspecific stabilization of the amphipathic N-terminal helix along the side of the Fab in a focus map. Although the pathway of the N-terminal extension is unlikely to be unique, the diagram does help us to understand why the increased prevalence of Fab moieties at the 2-fold hole (in r135+m25) is evidence for the increased anchoring of the amphipathic helix (residues 1-21) on the top surface of VP2, presumably stabilized by lower temperature and longer incubation before the antibody is introduced.

Figure S1: **Resolution and quality of maps.** (a.) Representative, raw micrographs of the datasets used in the analysis, (b.) Masked (continuous line) and unmasked (dotted line) Fourier shell correlation plots of m135 (red), r135 (green), h135 (cyan), r135+m25 (blue) and r135+m37 (purple). At a 0.143 cut-off level, the resolution estimates range from 2.8 to 3.6Å. (c.) Local resolution estimates in all the maps were calculated using Relion and the distribution of resolution values within in the masked region is plotted. (d.) In the best resolved dataset (m135), individual amino acid side chains are easily discriminated.

Figure S2: **Binding of anti-VP1 mAb to the VP1 N-terminus and infectivity of mAb released poliovirions** a.) The anti-VP1 antibody specifically recognizes and binds the N-terminus of VP1 only after the N-terminus has been externalized at 39˚C. Poliovirus particles were complexed with the antibody at room temperature or at 39˚C for 1.5 h and immunoprecipitated with magnetic Protein A coated beads. After thorough washing of the beads to remove unbound material, the samples were examined on SDS-PAGE gels. Lane 1, Ladder; lane 2, PV particles only; lane 3, antibody; lane 4, soluble fraction of antibody plus 160S PV after binding at RT; lane 5, pelleted fraction of antibody plus 160S PV after binding at RT; lane 6, soluble fraction of antibody plus 160S PV after binding at 39˚C; lane 7, pelleted fraction of antibody plus 160S PV after binding at 39˚C. Bottom panel, silver staining of the gel to enhance the relatively weak VP4 signal b.) Expanded poliovirus particles are infectious. Native (160S) poliovirus particles previously incubated with anti-VP1 antibody at room temperature or at 39˚C for 1.5 h were immunoprecipitated with magnetic Protein A coated beads. After thorough washing of the beads to remove unbound material, the beads were

freeze-thawed to release poliovirus particles. Released poliovirus was serially diluted and plated on naïve Vero cells. After 36 h of incubation at 37ºC, plaques were visualized by staining with crystal violet.

Figure S3: Visualising poliovirus VP1 N-terminus (a.) Asymmetric focused classes calculated for the r135+m25 dataset with percentage population per class. Class3 is depicted in Fig. 4b-c. (b.) Difference density, shown here in stereo, was calculated from previously published low-resolution reconstructions of poliovirus 135S particles, either untreated or treated with V8 protease, which cleaves at residue 31 of VP1. As a guide, we have superimposed an alpha carbon model of r135+m25. The blue alpha helix (putatively residues 1-21 of VP1) was fitted to a focused class of r135+m25 (as shown in Fig. 4d-e). Observe that the putative VP1 helix model, bound to the top of VP2, is similar in position and orientation to the previously reported difference map feature.

Table S1: Data collection parameters and refinement statistics. * The refinement statistics for the r135+m25 model are shown with the placeholder Fab and VP4 included as well as the capsid.

Table S2: List of residues that differ from the native structure. *Differently ordered residues are those residues that significantly differ in position from the native model (1HXS) following a least squares superposition of individual capsid proteins.

a.

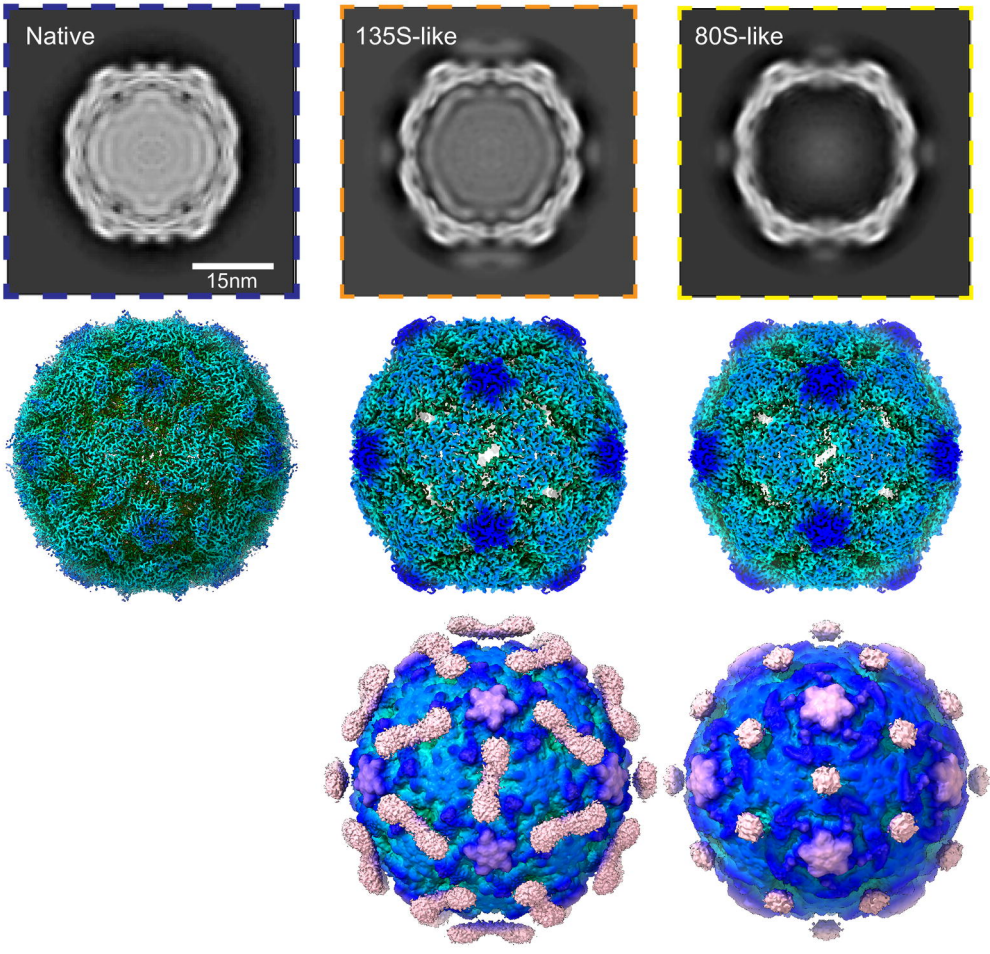

b.

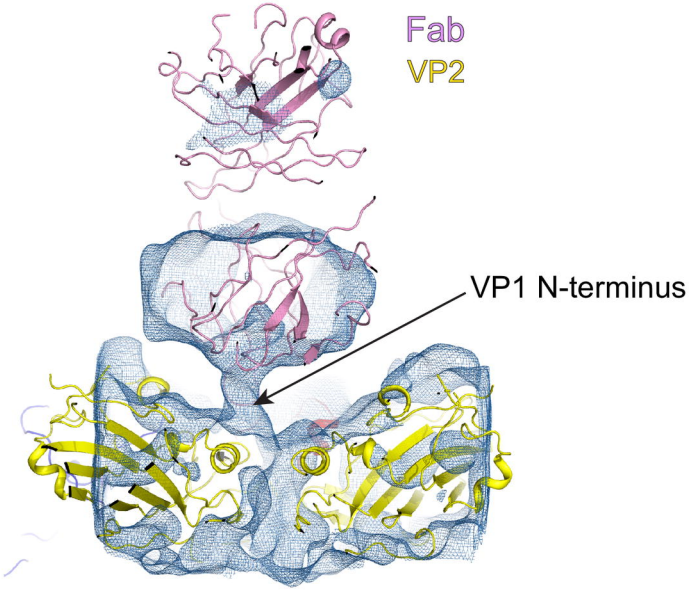

Figure 1: Anti-VP1 antibody trapped expanded particle

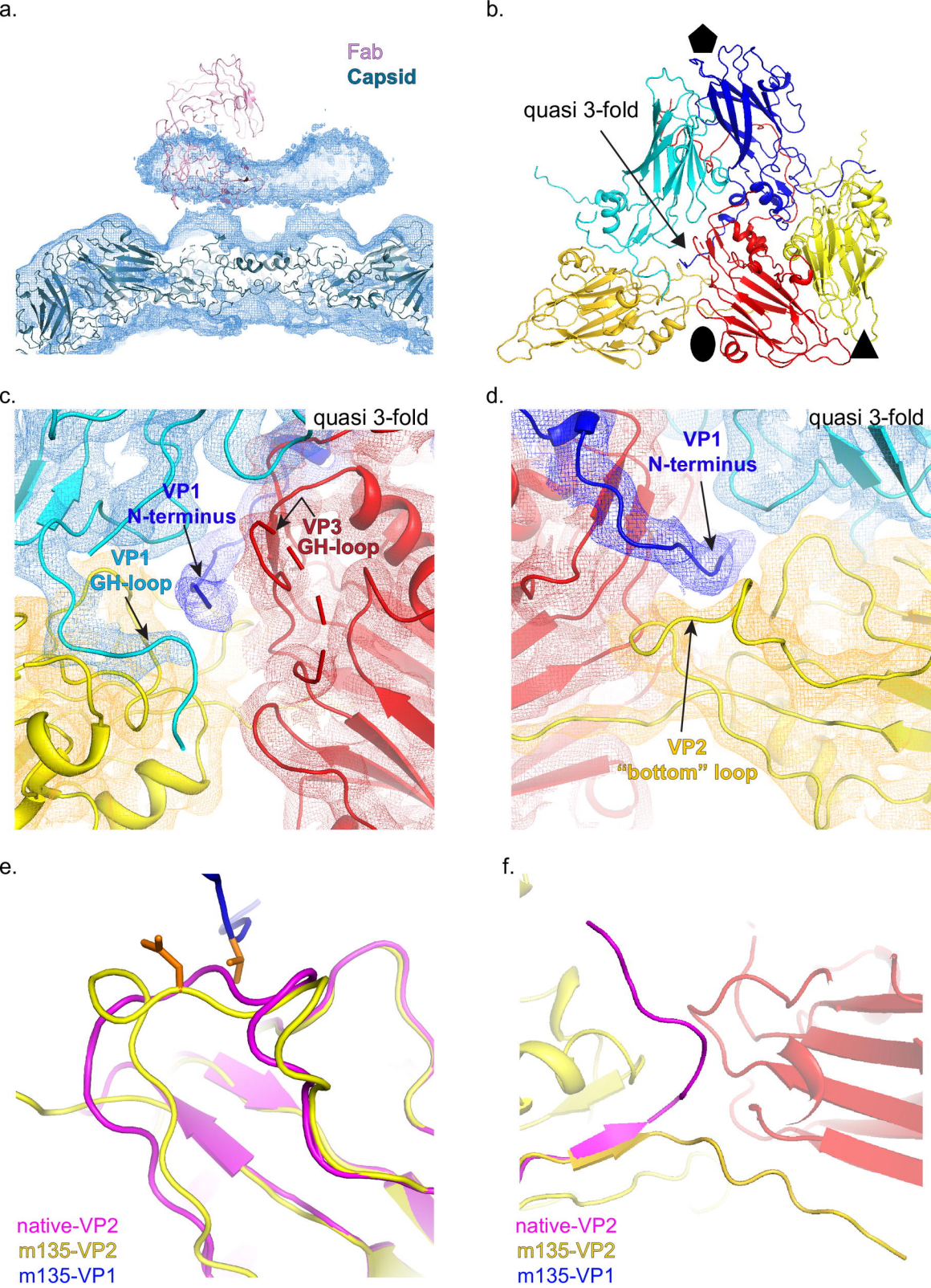

Figure 2: Anti-VP1 antibody trapped genome containing particle (m135) is similar to the canonical 135S particle.

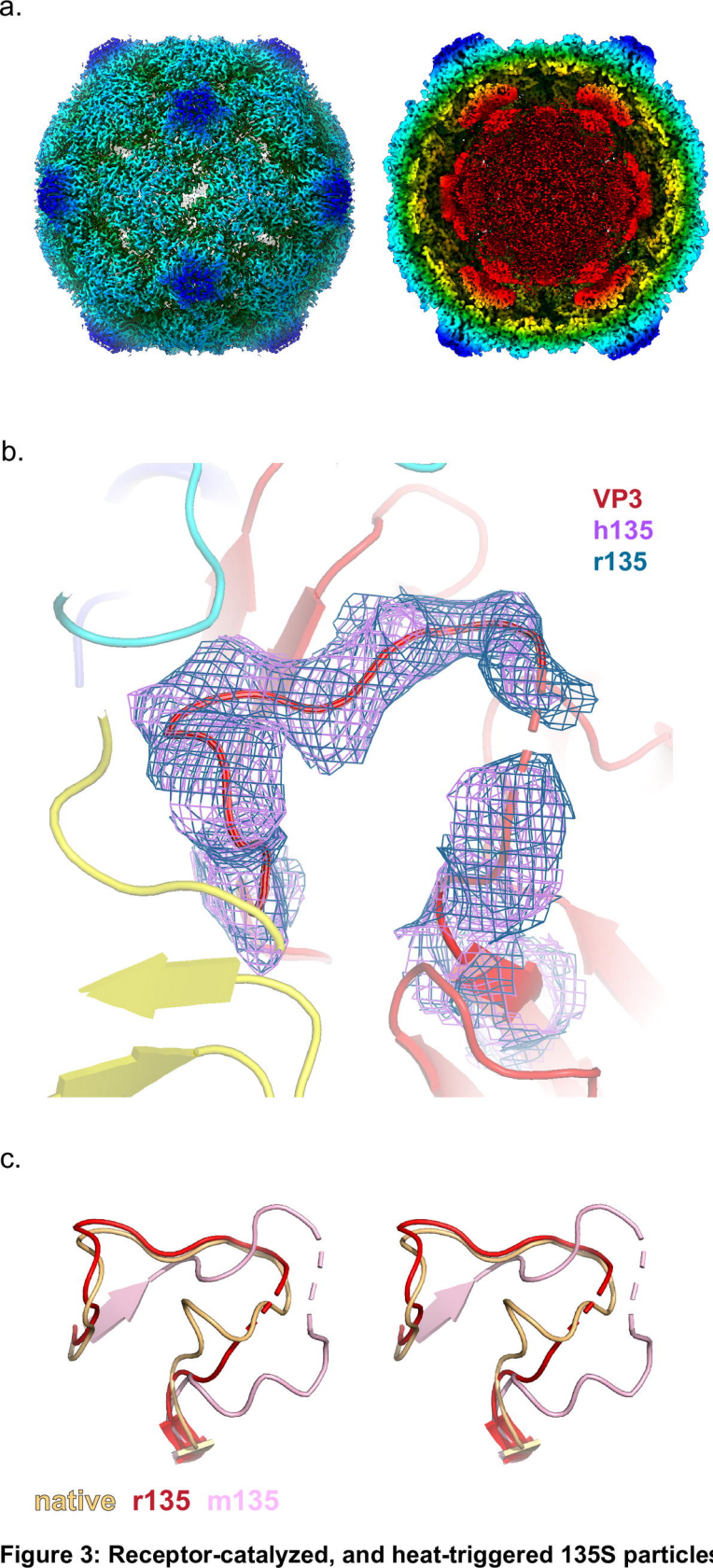

Figure 3: Receptor-catalyzed, and heat-triggered 135S particles (r/h135).

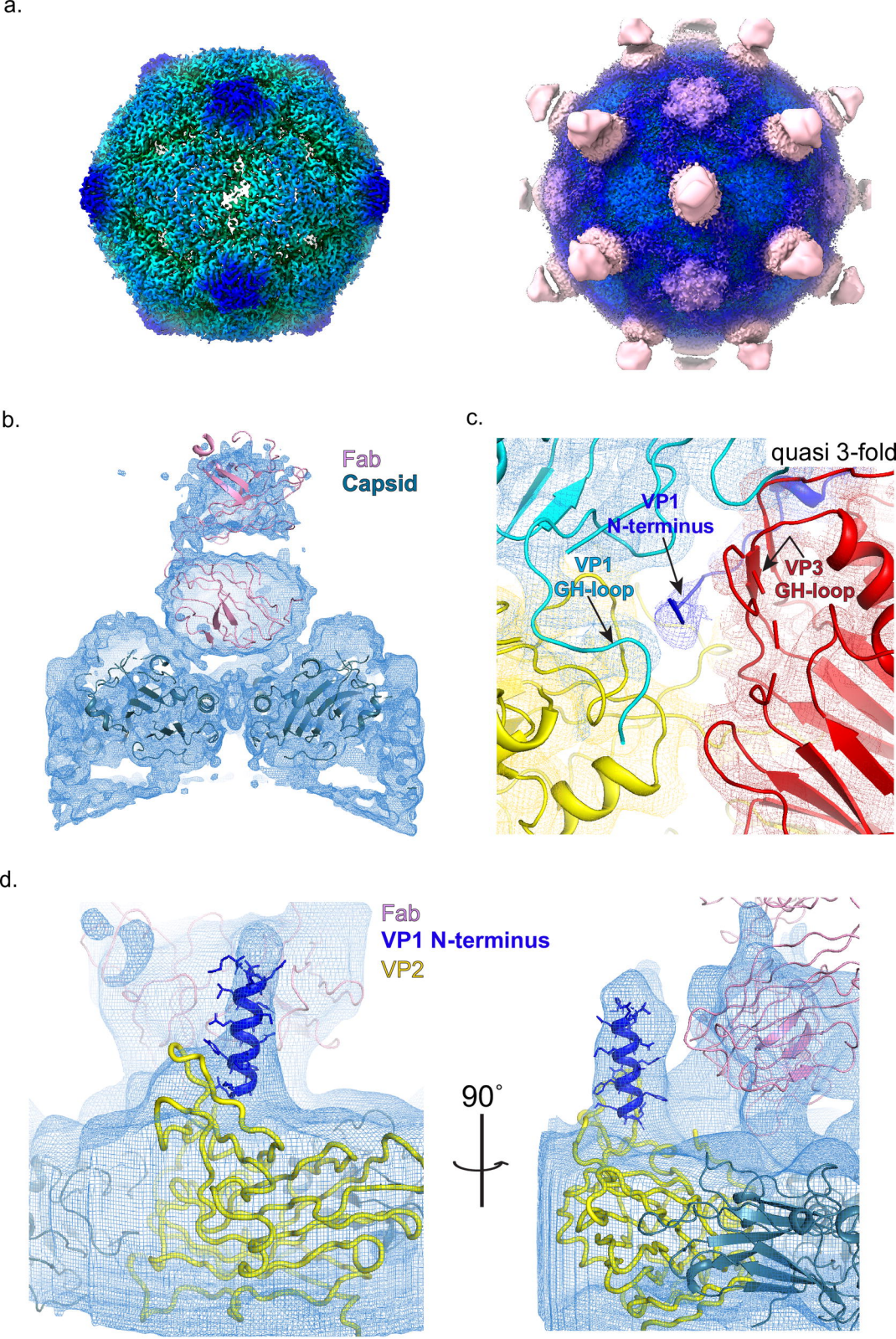

Figure 4: Receptor catalyzed 135S particle incubated with the anti-VP1 antibody at 25˚C (r135+m25).

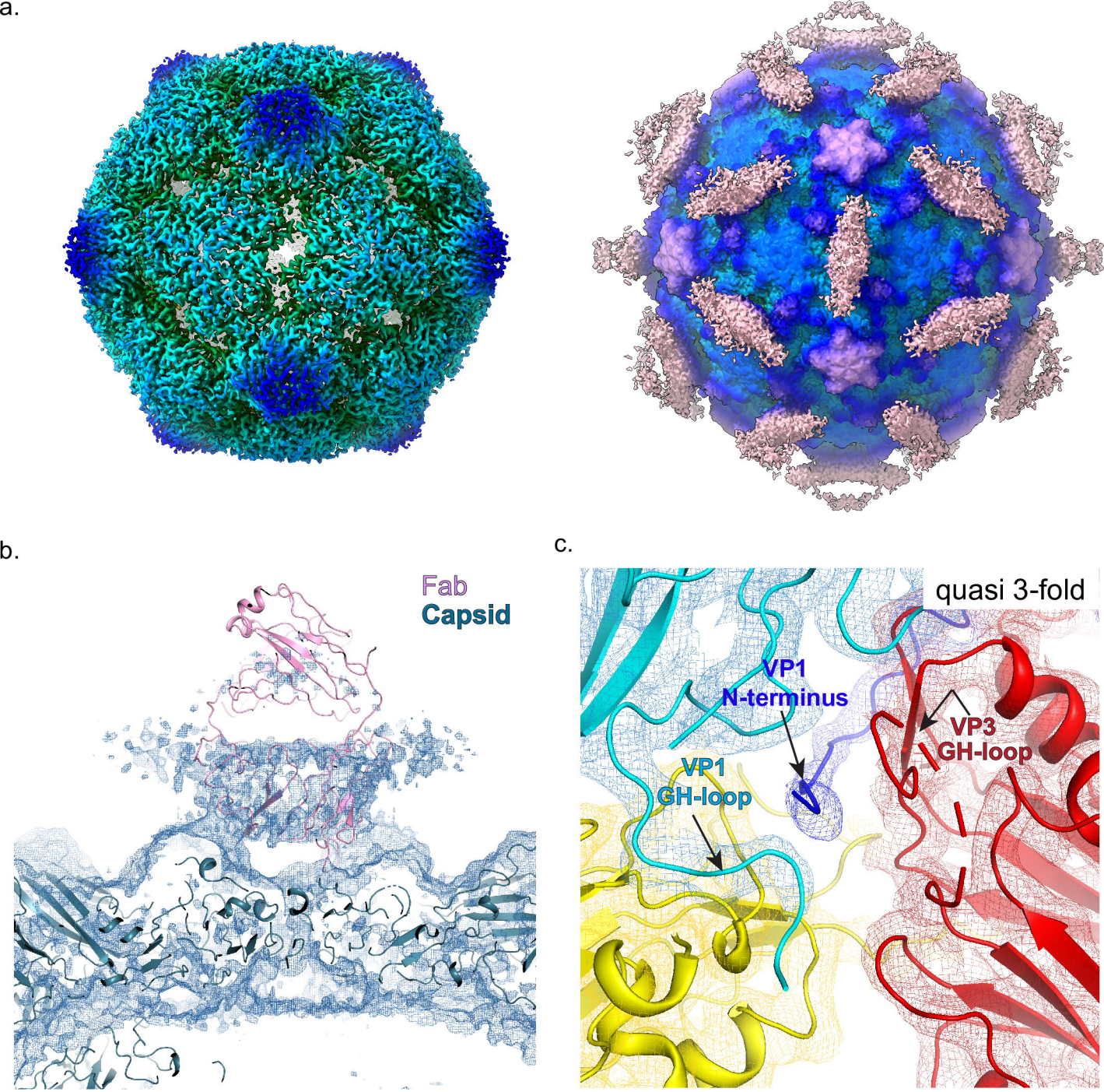

Figure 5: Receptor catalyzed 135S particle incubated with the anti-VP1 antibody at 37˚C (r135+m37)

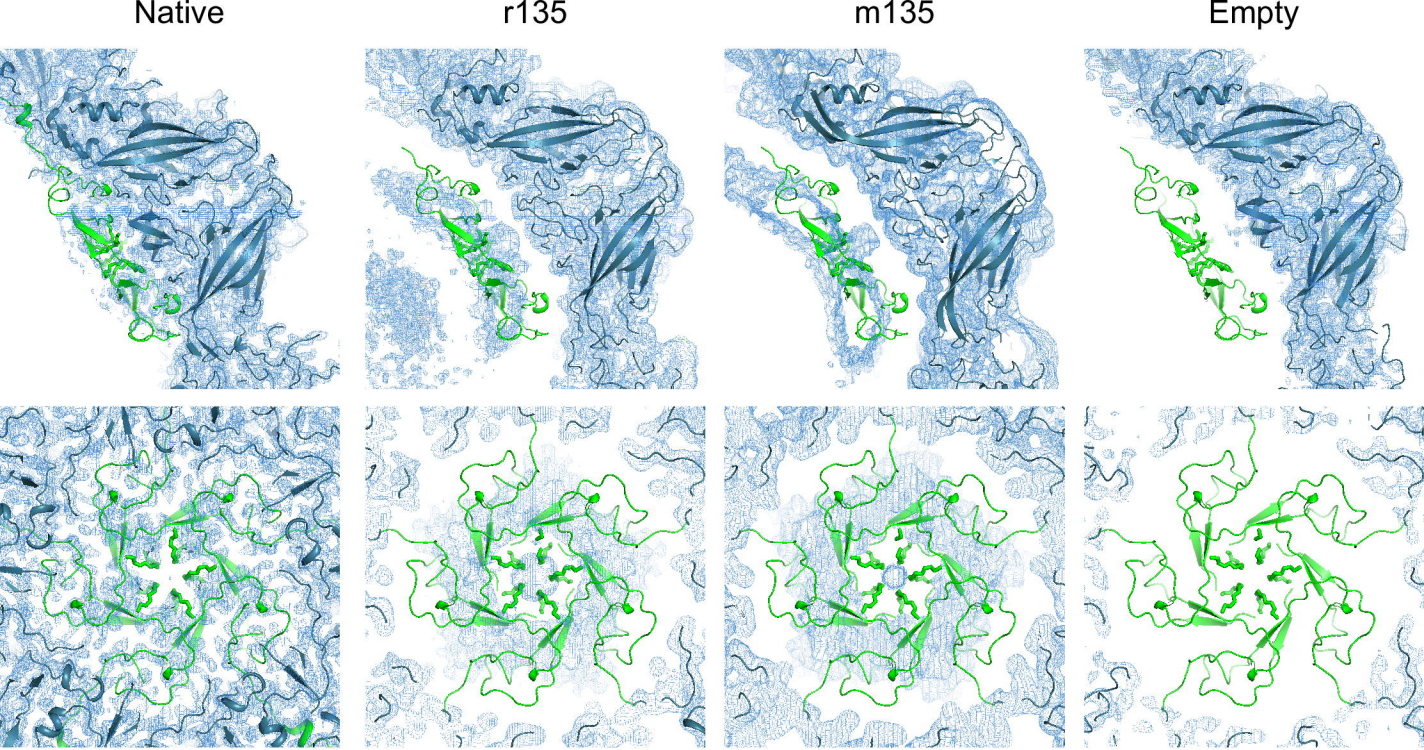

Figure 6: Location of VP4 before and after capsid expansion.

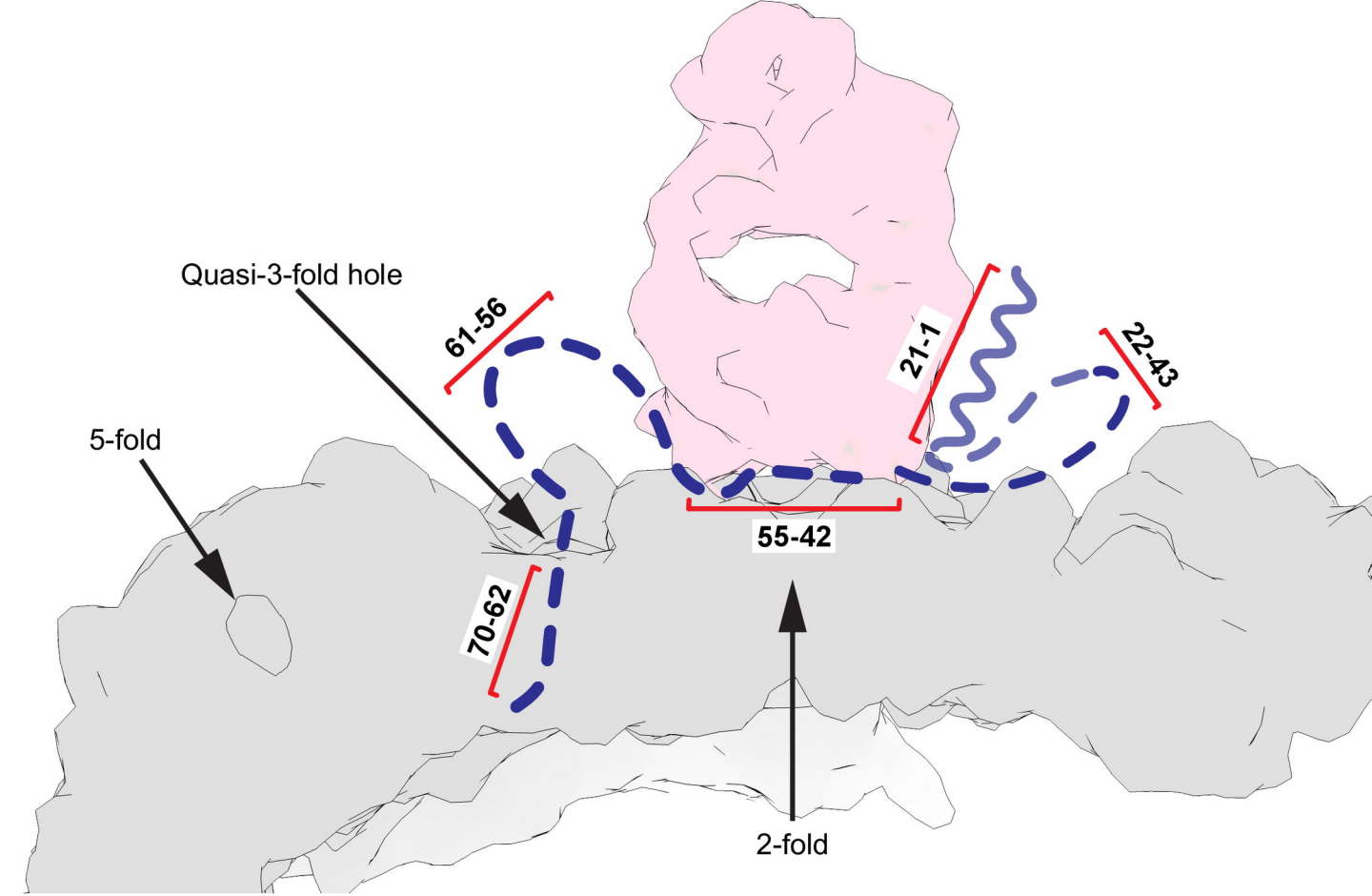

Figure 7: Schematic of VP1 N-terminal stabilization in the r135+m25 state.